

RESEARCH ARTICLE | FEBRUARY 11 2019

High resolution photoelectron imaging of boron-bismuth binary clusters: Bi_2B_n^- ($n = 2-4$)

Ling Fung Cheung ; Joseph Czekner ; G. Stephen Kocheril ; Lai-Sheng Wang 




J. Chem. Phys. 150, 064304 (2019)

<https://doi.org/10.1063/1.5084170>


 CHORUS



28 May 2024 16:40:20




Lock-in Amplifier



Zurich
Instruments

Find out more



Boxcar Averager

Boost Your Optics and Photonics Measurements





High resolution photoelectron imaging of boron-bismuth binary clusters: Bi_2B_n^- ($n = 2-4$)

Cite as: J. Chem. Phys. 150, 064304 (2019); doi: 10.1063/1.5084170

Submitted: 4 December 2018 • Accepted: 24 January 2019 •

Published Online: 11 February 2019



Ling Fung Cheung,  Joseph Czekner,  G. Stephen Kocheril,  and Lai-Sheng Wang^{a)} 

AFFILIATIONS

Department of Chemistry, Brown University, 324 Brook Street, Providence, Rhode Island 02912, USA

^{a)}Email: lai-sheng_wang@brown.edu

ABSTRACT

Bismuth boride is a heavy member of the III-V semiconductors. Although there have been some theoretical interests in this material, it has not been synthesized experimentally. Here, we report a high-resolution photoelectron imaging study on a series of boron-bismuth binary clusters, Bi_2B_n^- ($n = 2-4$), produced by laser vaporization of a B/Bi mixed target. Vibrationally resolved photoelectron spectra are obtained for all three clusters, and the measured vibrational and electronic information is used to compare with theoretical calculations to understand their structures and bonding. Bi_2B_2^- is found to be linear ($D_{\infty h}$, $^2\Pi_g$) with a B_2 unit and two terminal Bi atoms, while Bi_2B_3^- is found to be planar (C_{2v} , 1A_1), consisting of a B_3 triangle with two bridging Bi atoms. Interestingly, the spectra of Bi_2B_4^- reveal two co-existing isomers; both are found to be planar and contain a rhombus B_4 unit with two bridging Bi atoms in a *trans* (C_{2h} , 2A_u) and *cis* (C_{2v} , 2B_1) fashion separated only by 0.03 eV in energy. The interactions between the two Bi atoms and the B_n motifs are understood using chemical bonding analyses. This study shows that the Bi-B bonding is weak enough so that the B_n units maintain their structural integrity with the Bi atoms bonded to the cluster periphery only.

Published under license by AIP Publishing. <https://doi.org/10.1063/1.5084170>

I. INTRODUCTION

Bismuth boride is a heavy member of the III-V semiconductors, which are made of group III and V elements and form a class of important electronic and optical materials with wide industrial applications.¹ Although there have been increasing theoretical interests in bismuth boride (BBi),²⁻⁶ it has not been synthesized experimentally. Because of the large disparity in atomic size between B and Bi, bismuth boride is expected to exhibit interesting properties. There are no known bismuth-boron compounds, except a theoretical investigation on the substituent effects on the possible synthesis of a boron-bismuth triple bond.⁷ We have previously reported a photoelectron spectroscopy (PES) study on the gaseous BiBO^- species, which features a Bi-B single bond and a $\text{B}\equiv\text{O}$ boronyl unit.⁸ Recently, we have discovered a double-bonded $\text{Bi}=\text{B}$ species in Bi_2B^- ($[\text{Bi}=\text{B}=\text{Bi}]^-$) and a triple-bonded $\text{Bi}\equiv\text{B}$ species in BiB_2O^- ($[\text{Bi}\equiv\text{B}-\text{B}\equiv\text{O}]^-$).⁹ In the current work, we report a PES and theoretical study on a series of di-bismuth boride clusters, Bi_2B_n^- ($n = 2-4$).

Extensive studies on size-selected boron clusters have been carried out using joint experimental and theoretical investigations.¹⁰⁻¹⁶ The structural evolution and chemical bonding properties have been elucidated for boron clusters containing up to forty atoms. Small boron clusters have been found to be planar (2D) mostly with triangular lattices decorated with tetragonal, pentagonal, or hexagonal holes, which are critical for planarity. The discovery of the planar B_{36} cluster with a hexagonal hole led to the first experimental evidence of the viability of atom-thin 2D borons, named borophene,¹⁷ which has since been synthesized as a new class of synthetic 2D material.¹⁸ The B_{40} cluster was found to have a remarkable cage structure, becoming the first all-boron fullerene (borospherene) with D_{2h} symmetry.¹⁹ A number of metal-doped boron clusters have also been investigated by joint PES and theoretical studies, greatly expanding the structural diversity of nanoborons.²⁰⁻²⁴ The finding of the planar CoB_{18}^- cluster, in which the Co dopant becomes a part of the 2D plane, has led to the possibility of metal-laborophenes.²⁵⁻²⁸ Recently, we have found that di-lanthanide

octaboron clusters (Ln_2B_8^-) can form remarkable inverse sandwiches.²⁹

There have been few experimental studies of boron clusters doped by group V elements except B_nN^- ($n = 1-3$).³⁰⁻³² Computational studies have been reported on B_nN_2 ($n = 1-6$) and B_nP_2 ($n = 1-7$) clusters,^{33,34} as well as a joint experimental and theoretical study on the isoelectronic Bi_2Al_n ($n = 1-4$) clusters.³⁵ Extending our prior study on the bismuth-boron double bond and triple bond in Bi_2B^- and BiB_2O^- ,⁹ respectively, here we report an investigation on a series of di-bismuth boron clusters, Bi_2B_n^- ($n = 2-4$), using high resolution PE imaging and quantum chemical calculations. Vibrationally resolved PE spectra are obtained for all three clusters. The experimental electronic and vibrational information is compared with the theoretical results to elucidate the structures and bonding of these clusters. Bi_2B_2^- is found to be linear with two terminal Bi atoms forming double bonds with boron. Bi_2B_3^- is found to be planar and contains a B_3 triangle coordinated by two bridging Bi atoms. Two nearly degenerate planar isomers are observed for Bi_2B_4^- , consisting of a B_4 rhombus motif with the two Bi atoms coordinated in either the *trans* or *cis* configuration.

II. EXPERIMENTAL METHODS

The experiments were conducted using a high resolution PE imaging apparatus coupled to a laser vaporization supersonic cluster source, which has been described in detail previously.³⁶⁻³⁹ Briefly clusters were produced by focusing the second harmonic of a Nd:YAG laser onto a disk target made of a mixture of Bi and isotopically enriched ^{10}B powders. The laser-induced plasma formed inside the nozzle was cooled by a helium carrier gas seeded with 10% argon to initiate nucleation. The nascent clusters were entrained by the carrier gas and underwent a supersonic expansion to produce a cold cluster beam. Anionic clusters were extracted from the cluster beam perpendicularly into a time-of-flight mass spectrometer. The Bi_2B_n^- clusters of interest were mass selected before entering the interaction zone of the velocity-map imaging (VMI) detector. A second laser beam from an Nd:YAG laser or a Deyang Tech dye laser were used to photodetach electrons from the size-selected anions. Photoelectrons were focused onto a set of microchannel plates coupled with a phosphor screen and a charge-coupled device camera. A typical experiment at a given photon energy required about 50 000–100 000 laser shots to achieve reasonable signal-to-noise ratios. The VMI lens was calibrated using the photoelectron images of Au^- and Bi^- at different photon energies. The photoelectron images were analyzed using the maximum entropy method (MEVIR and MEVELER).⁴⁰ The typical energy resolution of the VMI detector is $\sim 0.6\%$ for high kinetic energy electrons and as low as 1.2 cm^{-1} for low kinetic energy electrons.³⁸

The PE images also yield information about the photoelectron angular distributions (PADs), which can be characterized by an anisotropy parameter (β). The differential cross section of the photoelectrons is described by

$$d\sigma/d\Omega = \sigma_{\text{Tot}}/4\pi[1 + \beta P_2(\cos\theta)], \quad (1)$$

where σ_{Tot} is the total cross section, P_2 is the second-order Legendre polynomial, and θ is the angle of the photoelectron relative to the laser polarization. The PAD is described by

$$I(\theta) \sim [1 + \beta P_2(\cos\theta)], \quad (2)$$

where β has a value ranging from -1 to 2 . This model works well for single photon transitions from randomly oriented particles. Since photons carry one unit of angular momentum ($l = \pm 1$), the outgoing photoelectrons will have the same change in their angular momentum. For example, if an electron is detached from an s atomic orbital ($l = 0$), the outgoing photoelectron will have $l = 1$ (pure p -wave) with $\beta = 2$. It is not a trivial process to interpret the β value for ionization from a molecular orbital (MO) because MOs are linear combinations of atomic orbitals. Nonetheless, the values of β can be used to qualitatively assess the symmetries of the molecular orbitals involved in the photodetachment process.⁴¹

III. THEORETICAL METHODS

Global minimum searches for the Bi_2B_n^- ($n = 2-4$) clusters were done using the simulated annealing algorithm coupled with density functional theory (DFT) geometry optimization.⁴²⁻⁴⁵ About 200–300 structures were generated for each cluster and were first optimized at the PBE/LAN2DZ level of theory.^{46,47} Further geometric optimizations and vibrational analyses were carried out, for the top low-lying isomers within 1 eV of the global minima, using the TPSSH functional with the aug-cc-pVTZ basis set for B and aug-cc-pVTZ-pp basis set with the relativistic pseudopotentials (ECP60MDF) for Bi.⁴⁸⁻⁵⁰ All calculations were performed in Gaussian 09.⁵¹

The adiabatic detachment energy (ADE) for the ground state was calculated as the energy difference between the optimized anion and neutral with zero-point energy corrections, which represents the electron affinity (EA) for the neutral cluster. The ADEs for the clusters with different spin multiplicities were also calculated. The vertical detachment energies (VDEs) for the higher excited states were computed using time-dependent density functional theory (TD-DFT) at the anion geometry. The adaptive natural density partitioning (AdNDP) method was used for chemical bonding analyses.⁵² Franck-Condon (FC) factors for the ground state transitions were calculated using the ezSpectrum v3.0 program⁵³ and the theoretical structures and frequencies. The FC factors were fitted with Gaussian functions to produce simulated spectra.

IV. EXPERIMENTAL RESULTS

A. The PE images and spectra of Bi_2B_2^-

Figure 1 shows the PE images and their corresponding spectra for Bi_2B_2^- at four different photon energies. The sharp peak labeled X denotes the 0–0 transition and its peak position in the highest resolution spectrum [Fig. 1(a)] defines the

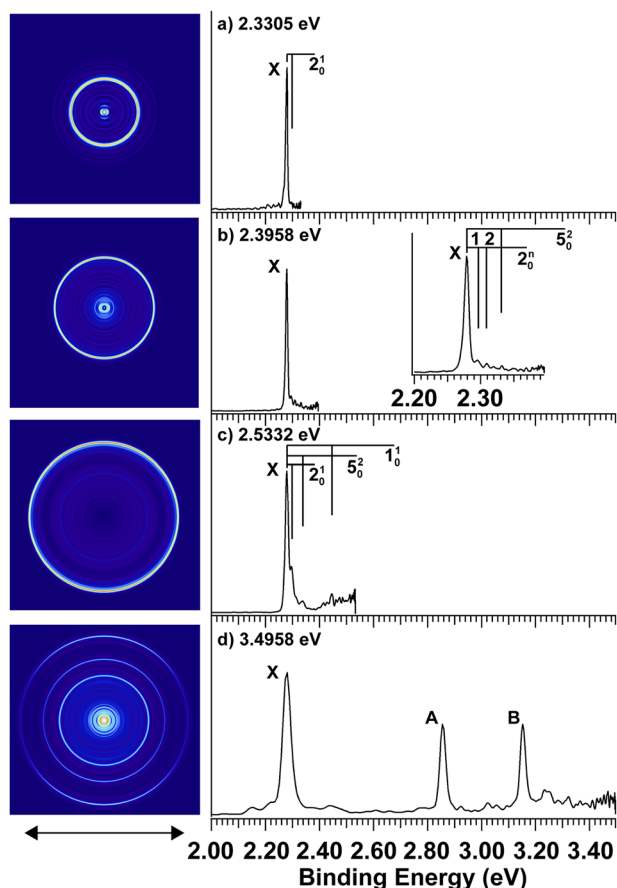


FIG. 1. Photoelectron images and spectra of Bi_2B_2^- at four photon energies: (a) 2.3305 eV (532.00 nm), (b) 2.3958 eV (517.51 nm), (c) 2.5332 eV (489.43 nm), and (d) 3.4958 eV (354.67 nm). The vertical lines represent vibrational structures, and the double arrow below the images indicates the laser polarization.

EA of Bi_2B_2 to be 2.2783 eV (Table I). Vibrational information for Bi_2B_2 was obtained from the spectra taken at 2.3958 eV [Fig. 1(b)] and 2.5332 eV [Fig. 1(c)]. Two vibrational progressions with frequencies of $125 \pm 25 \text{ cm}^{-1}$ and $216 \pm 12 \text{ cm}^{-1}$ were

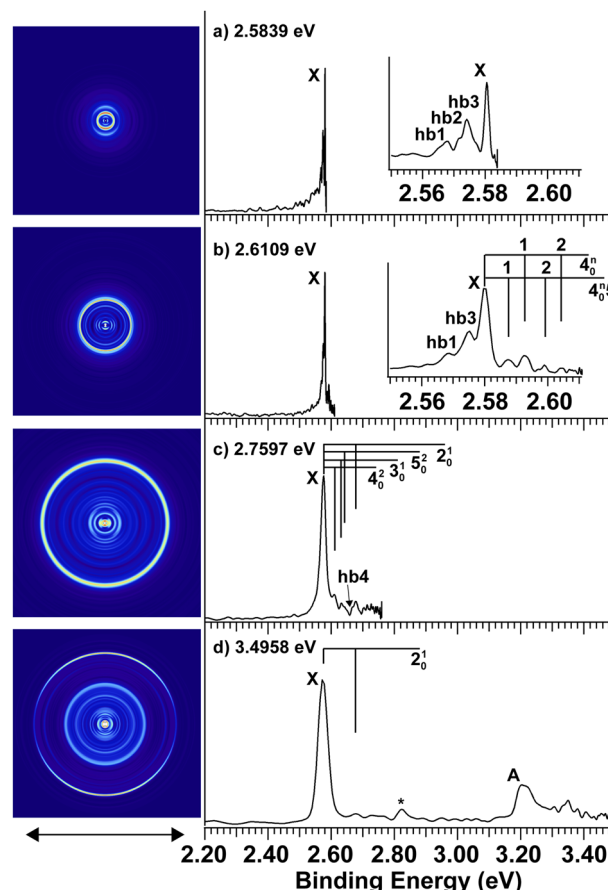


FIG. 2. Photoelectron images and spectra of Bi_2B_3^- at four photon energies: (a) 2.5839 eV (479.83 nm), (b) 2.6109 eV (474.87 nm), (c) 2.7597 eV (449.27 nm), and (d) 3.4958 eV (354.67 nm). The vertical lines represent vibrational structures, and the double arrow below the images indicates the laser polarization. "hb" stands for vibrational hot bands.

observed in Fig. 1(b) and denoted with vertical lines (see the inset). Another progression was found to be $1345 \pm 35 \text{ cm}^{-1}$ in Fig. 1(c). The spectrum taken at 3.4958 eV [Fig. 1(d)] shows

TABLE I. Experimental and theoretical binding energies (BE) in eV of the observed PES bands of Bi_2B_2^- and the corresponding electronic states and MO configurations of Bi_2B_2 , as well as the observed and calculated vibrational frequencies in cm^{-1} and symmetries.

Band	BE (expt.)	BE (theor)	Vibrational mode	Freq. (expt.)	Frequency (theor)	Symmetry	Final state and MO configuration
X	2.2783(54) ^a	2.32 ^a	ν_1	1345(35)	1377	Σ_g^-	$3\Sigma_g^- \dots 1\sigma_g^2 1\sigma_u^2 2\sigma_g^2 2\sigma_u^2 3\sigma_g^2 1\pi_u^4 1\pi_g^2$
			ν_2	125(25)	123	Σ_g^-	
			ν_5	216(12) ^b	272	Π_g	
A	2.87(2) ^c	...					$1\Sigma_g^- \dots 1\sigma_g^2 1\sigma_u^2 2\sigma_g^2 2\sigma_u^2 3\sigma_g^2 1\pi_u^4 1\pi_g^2$
B	3.15(2) ^c	3.05 ^c					$1\Delta_g \dots 1\sigma_g^2 1\sigma_u^2 2\sigma_g^2 2\sigma_u^2 3\sigma_g^2 1\pi_u^4 1\pi_g^2$

^aADE.

^bOnly transitions of even quanta of this vibrational mode are allowed by symmetry. This value is half of the measured separation from the 0-0 transition (see Fig. 1 and Table S1 of the supplementary material).

^cVDE.

TABLE II. Experimental and theoretical binding energies (BE) in eV of the observed PES bands of Bi_2B_3^- and the corresponding electronic states and MO configurations of Bi_2B_3 , as well as the observed and calculated vibrational frequencies in cm^{-1} and symmetries.

Band	BE (expt.)	(Theor)	Vibrational mode	Frequency (exp.)	Frequency (theor)	Symmetry	Final state and MO configuration
X	2.5805(9) ^a	2.43 ^a	ν_2	786(41)	886	A_1	$^2A_2 \dots 1a_1^2 1b_2^2 2a_1^2 3a_1^2 2b_2^2 1b_1^2 4a_1^2 3b_2^2 5a_1^2 1a_2^1$
			ν_3	415(23)	342	A_1	
			ν_4	96(7)	112	A_1	
			ν_5	251(19) ^b	266	A_2	
A	3.21(3) ^c	3.16 ^c					$^2A_1 \dots 1a_1^2 1b_2^2 2a_1^2 3a_1^2 2b_2^2 1b_1^2 4a_1^2 3b_2^2 5a_1^1 1a_2^2$

^aADE.^bOnly transitions of even quanta of this vibrational mode are allowed by symmetry. This value is half of the measured separation from the 0-0 transition (see Fig. 2 and Table S2 of the [supplementary material](#)).^cVDE.

two additional peaks, labeled A and B, which should correspond to the excited electronic states of Bi_2B_2 (Table I). The peak positions of all the observed vibrational features and their assignments are given in Table SI of the [supplementary material](#) (also see Fig. S1 of the [supplementary material](#) for the peak labels).

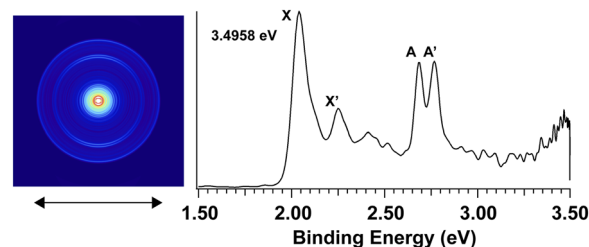
B. The PE images and spectra of Bi_2B_3^-

The PE images and spectra of Bi_2B_3^- at four different photon energies are shown in Fig. 2. The sharp peak labeled X located at 2.5805 eV in Fig. 2(a) defines the 0-0 transition and the EA of Bi_2B_3 (Table II). In addition, there are several peaks at lower binding energies labeled hb1-hb3 due to vibrational hot bands [see the inset in Fig. 1(a)]. In the 2.6109 eV spectrum [Fig. 2(b)], two sets of nearly equally spaced peaks are denoted with vertical lines ($92 \pm 8 \text{ cm}^{-1}$ for the first progression and $96 \pm 7 \text{ cm}^{-1}$ for the second). In the spectrum taken at 2.7597 eV [Fig. 2(c)], two more vibrational features were observed with shifts of $415 \pm 23 \text{ cm}^{-1}$ (3_0^1) and $786 \pm 41 \text{ cm}^{-1}$ (2_0^1) above peak X. There are two shoulders right next to these two peaks. By fitting with Gaussian functions, we found the positions of the two shoulders to be $502 \pm 38 \text{ cm}^{-1}$ (5_0^2) and $690 \pm 13 \text{ cm}^{-1}$ (hb4) above peak X. Finally, one additional peak (A) was observed in the 3.4958 eV spectrum [Fig. 2(d)] at a binding energy of 3.21 eV, which should be an electronic excited state of Bi_2B_3 (Table II). The small peak labeled with an asterisk is $1974 \pm 76 \text{ cm}^{-1}$ above peak X. This peak does not correspond to any vibrational excitation in the ground state

and is likely due to a multi-electron process, as observed previously in the PE spectrum of B_3^- .⁵⁴ The binding energies of all the vibrational peaks and their assignments are given in Table SII of the [supplementary material](#) (also see Fig. S2 of the [supplementary material](#) for all the peak labels).

C. The PE images and spectra of Bi_2B_4^-

The PE spectrum of Bi_2B_4^- is much more complicated, as shown in Fig. 3, where four broad bands (X, X', A, and A') are observed. It turned out that there were two nearly degenerate isomers present in the Bi_2B_4^- cluster beam (*vide infra*): the bands X and X' are the ground state transitions of the two isomers, and bands A and A' correspond to the excited states of the neutrals of the two isomers. The detachment energies for

**FIG. 3.** Photoelectron image and spectrum of Bi_2B_4^- at 3.4958 eV (354.67 nm). The double arrow below the image indicates the laser polarization.**TABLE III.** Experimental and theoretical binding energies (BE) in eV of the observed PES bands of Bi_2B_4^- and the corresponding electronic states and MO configurations of Bi_2B_4 , as well as the observed and calculated vibrational frequencies in cm^{-1} and symmetries.

Band	BE (expt.)	(Theor)	Vibrational mode	Frequency (expt.)	Frequency (theor)	Symmetry	Final state and MO configuration
X	2.0102(4) ^a	1.90 ^a	ν_5	125(2)	137	A_g	$^1A_g \dots 1a_g^2 1b_u^2 2a_g^2 2b_u^2 3b_u^2 1a_u^2 3a_g^2 4a_g^2 4b_u^2 5a_g^2 1b_g^2$
X'	2.2510(5) ^a	2.20 ^a	ν_4	67(3)	77	A_1	$^1A_1 \dots 1a_1^2 1b_2^2 2a_1^2 2b_2^2 3a_1^2 1b_1^2 4a_1^2 3b_2^2 5a_1^2 4b_2^2 1a_2^2$
			ν_5	379(5)	414	A_1	
A	2.69(3) ^b	2.57 ^b					$^3B_u \dots 1a_g^2 1b_u^2 2a_g^2 2b_u^2 3b_u^2 1a_u^2 3a_g^2 4a_g^2 4b_u^2 5a_g^2 1b_g^2 1a_u^1$
A'	2.77(4) ^b	2.66 ^b					$^3B_2 \dots 1a_1^2 1b_2^2 2a_1^2 2b_2^2 3a_1^2 1b_1^2 4a_1^2 3b_2^2 5a_1^2 4b_2^2 1a_2^2 1b_1^1$

^aADE.^bVDE.

the four bands are given in Table III, where the values for X and X' are obtained from the high-resolution spectra presented in Figs. 4 and 5.

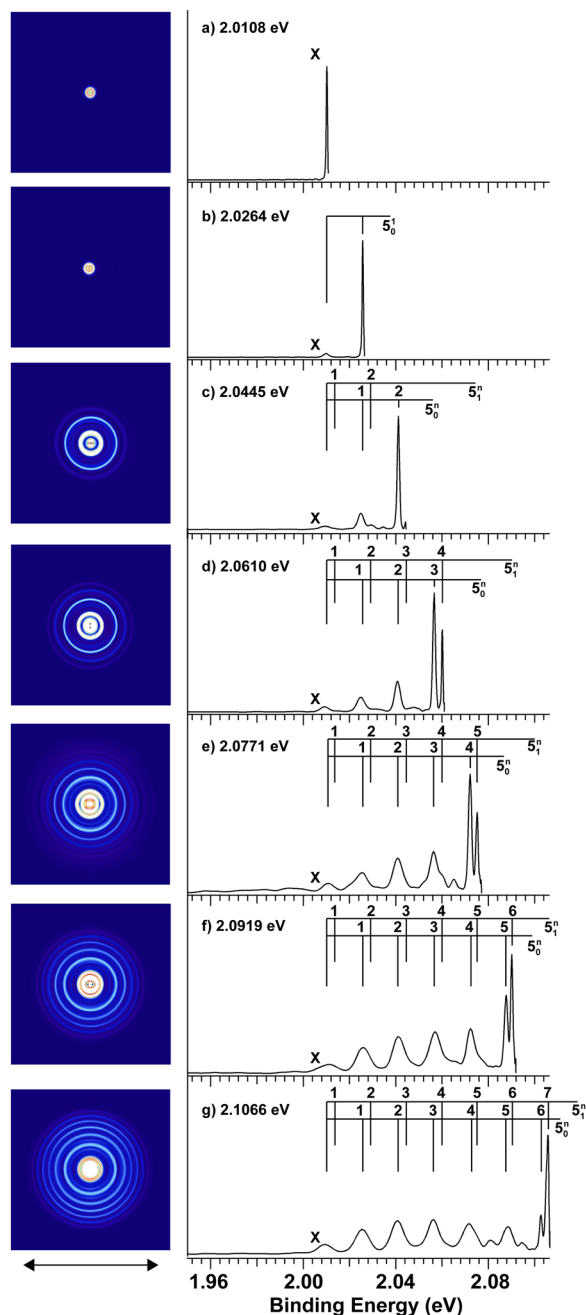


FIG. 4. High resolution photoelectron images and spectra of the X band of Bi_2B_4^- at seven photon energies: (a) 2.0108 eV (616.60 nm), (b) 2.0264 eV (611.83 nm), (c) 2.0445 eV (606.43 nm), (d) 2.0610 eV (601.56 nm), (e) 2.0771 eV (596.92 nm), (f) 2.0919 eV (592.69 nm), and (g) 2.1066 eV (588.55 nm). The vertical lines represent the vibrational structures, and the double arrow below the images indicates the laser polarization.

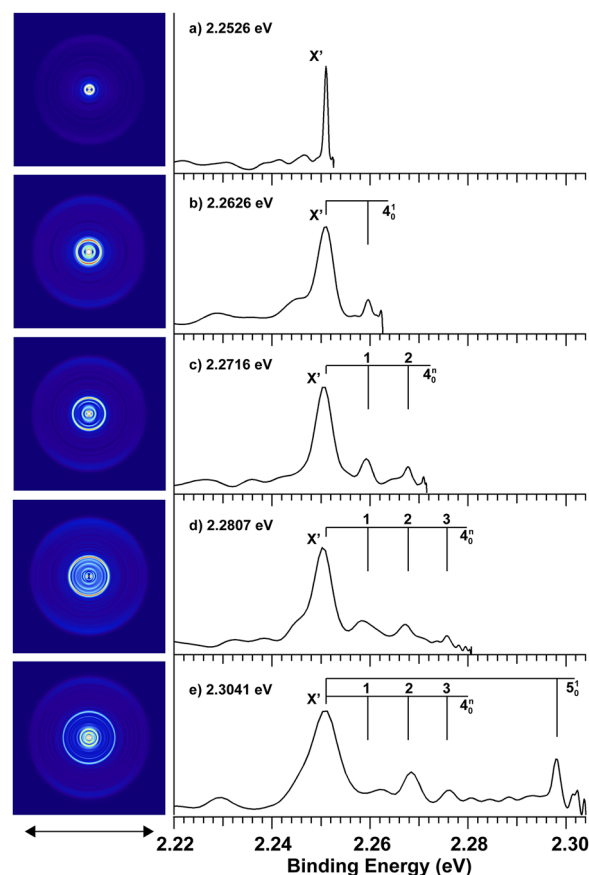


FIG. 5. High resolution photoelectron spectra and images of the X' band of Bi_2B_4^- at five photon energies: (a) 2.2526 eV (550.41 nm), (b) 2.2626 eV (547.97 nm), (c) 2.2716 eV (545.81 nm), (d) 2.2807 eV (543.62 nm), and (e) 2.3041 eV (537.11 nm). The vertical lines represent vibrational structures, and the double arrow below the images indicates the laser polarization.

High-resolution spectra were taken for band X at a series of low photon energies from 2.0108 eV [Fig. 4(a)] to 2.1066 eV [Fig. 4(g)], revealing a broad vibrational progression. The ADE of band X is accurately measured as 2.0102 eV from the near threshold detachment [Fig. 4(a)]. Furthermore, each peak in the progression was found to be a doublet, as seen in Figs. 4(d)–4(g). The second peak of the doublet was cut off in Figs. 4(a)–4(c) because the photon energies used were too close to the lower binding energy peak of the first progression. The spacing of the two vibrational progressions, as shown by the vertical lines, is the same ($125 \pm 2 \text{ cm}^{-1}$ for the first progression and $122 \pm 5 \text{ cm}^{-1}$ for the second), indicating that the two progressions represent the same neutral vibrational mode. In addition, the peaks near threshold in each spectrum are much sharper and appear more intense, but the integrated intensities are approximately consistent with the overall Franck-Condon profile of band X.

Figure 5 shows the high resolution PE spectra for band X'. As shown in Fig. 3, there is some overlap between bands

X and X', i.e., transitions to higher vibrational levels of band X extend into band X'. Despite this complication, we were able to observe clearly the 0-0 transition of band X' at 2.2510 eV (Table III), as shown in Fig. 5(a). Several weak peaks observed at higher binding energies are assigned to two vibrational progressions, as denoted by the vertical lines in Figs. 5(b)–5(e). The frequencies of the two progressions are measured to be $67 \pm 3 \text{ cm}^{-1}$ and $379 \pm 5 \text{ cm}^{-1}$. The peak positions of all the observed vibrational features for bands X and X' are given in Table SIII of the [supplementary material](#) (see Figs. S3 and S4 of the [supplementary material](#) for the peak labels).

V. THEORETICAL RESULTS

Theoretical calculations were carried out to understand the electronic and vibrational structures of Bi_2B_n^- ($n = 2-4$) and their corresponding neutrals upon electron detachment. Three low-lying structures were found for each cluster anion within 1 eV of the global minimum, as given in Fig. S5 of the [supplementary material](#). These structures were further optimized at the TPSSh/Bi/aug-cc-pVTZ-pp/B/aug-cc-pVTZ level of theory and relatively small energy changes were found. The global minima at the TPSSh level and their corresponding neutrals, as well as a low-lying isomer within 0.8 eV of the global minimum and their corresponding neutrals, are presented in Fig. 6. The computed vibrational frequencies of these isomers are given in Table SIV of the [supplementary material](#).

A. Bi_2B_2^- and Bi_2B_2

The global minimum of Bi_2B_2^- was found to be linear with a Bi–B–Bi configuration [2.I-a in Fig. 6(a)]. The electronic configuration of isomer 2.I-a is $1\sigma_g^2 1\sigma_u^2 2\sigma_g^2 2\sigma_u^2 3\sigma_g^2 1\pi_u^4 1\pi_g^3$ with a $^2\Pi_g$ term and a $^2\Pi_{g3/2}$ spin-orbit (SO) ground state. Since the SO splitting for the $^2\Pi_g$ term is expected to be large on the basis of the previous observation of 0.54 eV in Bi_2B ,⁹ the $^2\Pi_{g1/2}$ SO-excited state was not expected to be populated. Removing an electron from the $1\pi_g$ highest occupied molecular orbital (HOMO) yields the $^3\Sigma_g^-$ ground state for the neutral linear isomer, and its optimized geometry is displayed in Fig. 6(a) (isomer 2.I-n).

The next lowest energy isomer for Bi_2B_2^- (2.II-a) is 0.26 eV higher in energy than the linear isomer, and it has a rhombus structure (D_{2h}) with each Bi atom bridging the two B atoms. The corresponding neutral of the rhombus isomer (2.II-n) was found to be 0.16 eV more stable than the linear isomer 2.I-n [Fig. 6(a)]. However, since the anionic isomer 2.II-a was predicted to be 0.26 eV higher in energy than isomer 2.I-a, the rhombus anion was not expected to be populated in the cluster beam. The calculated electron binding energies of the linear Bi_2B_2^- global minimum and the vibrational frequencies of the corresponding neutral are compared with the experimental data in Table I.

B. Bi_2B_3^- and Bi_2B_3

For Bi_2B_3^- , a planar structure with two Bi atoms bonded to a triangular B_3 unit was found to be the global minimum

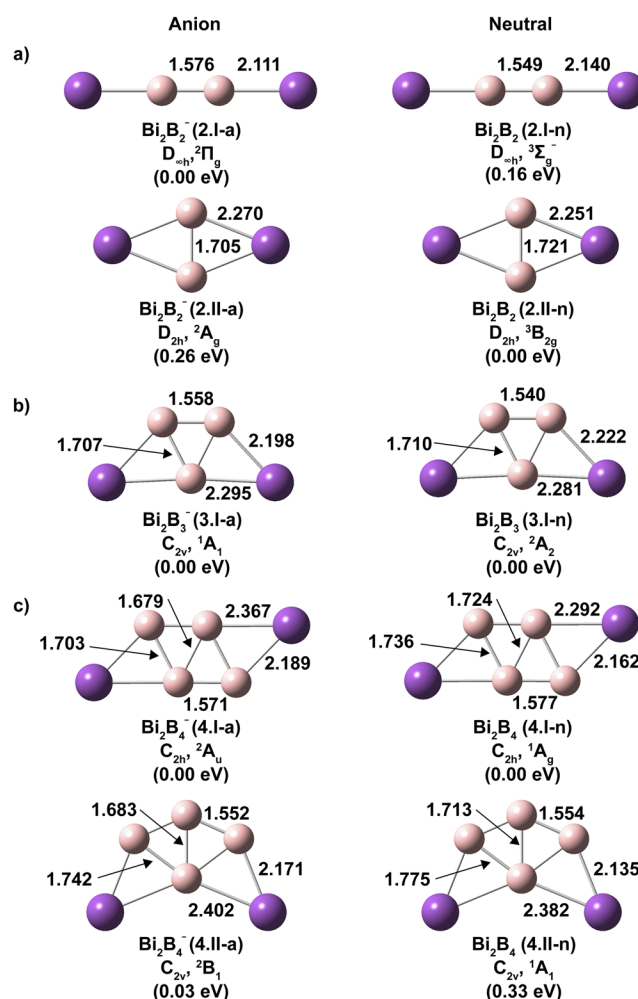


FIG. 6. The global minima and low-lying structures of (a) Bi_2B_2^- , (b) Bi_2B_3^- , (c) Bi_2B_4^- , and their corresponding neutrals optimized at the TPSSh/Bi/aug-cc-pVTZ-pp/B/aug-cc-pVTZ level of theory. Bond lengths are given in Å.

[3.I-a in Fig. 6(b)]. It has C_{2v} symmetry with a closed-shell electron configuration: $1a_1^2 1b_2^2 2a_1^2 3a_1^2 2b_2^2 1b_1^2 4a_1^2 3b_2^2 5a_1^2 1a_2^2$. Removing an electron from the $1a_2$ HOMO gives the lowest energy neutral state (isomer 3.I-n). Its optimized geometry is also presented in Fig. 6(b). No other low-lying isomers were found, suggesting its high stability. The closest-lying isomer has a linear configuration, which is 0.97 eV higher in energy at the TPSSh level (Fig. S5 of the [supplementary material](#)). The calculated electron binding energies of the C_{2v} global minimum of Bi_2B_3^- and the vibrational frequencies of the corresponding neutral are compared with the experimental data in Table II.

C. Bi_2B_4^- and Bi_2B_4

Two close-lying planar isomers were found for Bi_2B_4^- , as displayed in Fig. 6(c) (4.I-a and 4.II-a). These two

isomers have a calculated energy difference of only 0.03 eV, so they are essentially degenerate within the computational accuracy. Both isomers contain a rhombus B_4 motif with the two Bi atoms bridge-bonded in either a *trans* (4.I-a, C_{2h}) or *cis* (4.II-a, C_{2v}) fashion. The *trans* isomer was found to be slightly lower in energy with an electron configuration of $1a_g^2 1b_u^2 2a_g^2 2b_u^2 3b_u^2 1a_u^2 3a_g^2 4a_g^2 4b_u^2 5a_g^2 1b_g^2 2a_u^1$ and a 2A_u state. The corresponding neutral (4.I-n) has the same symmetry and is closed-shell (1A_g state) by removal of the electron in the $2a_u$ HOMO. The *cis* isomer of $Bi_2B_4^-$ has an electron configuration of $1a_1^2 1b_2^2 2a_1^2 2b_2^2 3a_1^2 1b_1^2 4a_1^2 3b_2^2 5a_1^2 4b_2^2 1a_2^2 2b_1^1$ with a 2B_1 electronic state. Removing an electron from the $2b_1$ HOMO yields the 1A_1 neutral ground state. However, the neutral *cis* isomer (4.II.n) was found to be 0.33 eV higher in energy than the *trans* neutral isomer. There were no other low-lying isomers for $Bi_2B_4^-$ within 1.0 eV of the C_{2h} global minimum. The next isomer was found to be more than 1 eV higher in energy (Fig. S5 of the [supplementary material](#)). The calculated electron binding energies of the two nearly degenerate isomers of $Bi_2B_4^-$ and the vibrational frequencies of their corresponding neutrals are compared with the experimental data in [Table III](#).

VI. DISCUSSION

A. Spectral assignments and comparison between experiment and theory

1. $Bi_2B_2^-$

The intense 0-0 transition for band X along with only a weak and short vibrational progression in the PE spectra of $Bi_2B_2^-$ (Fig. 1) suggests that the $Bi_2B_2^-$ anion is likely to have high symmetry with a relatively small geometry change upon electron detachment. The calculated ADE of the linear isomer 2.I-a for the $^3\Sigma_g^- \leftarrow ^2\Pi_g$ ground state detachment transition was 2.32 eV, in good agreement with the measured ADE of band X (2.2783 eV, [Table I](#)). The $1\pi_g$ HOMO of the linear structure (Fig. S6a of the [supplementary material](#)) is mainly of Bi 6p character with weak Bi-B π bonding and B-B anti-bonding characters, consistent with the minor geometry change between the anion and neutral ground state [Fig. 6(a)] and the short vibrational progression in the PE spectra. The calculated frequencies of the B-B and Bi-B symmetric stretching modes for the $^3\Sigma_g^-$ neutral state, 1377 cm^{-1} and 123 cm^{-1} , respectively [Fig. 7(a)], also agreed well with the measured

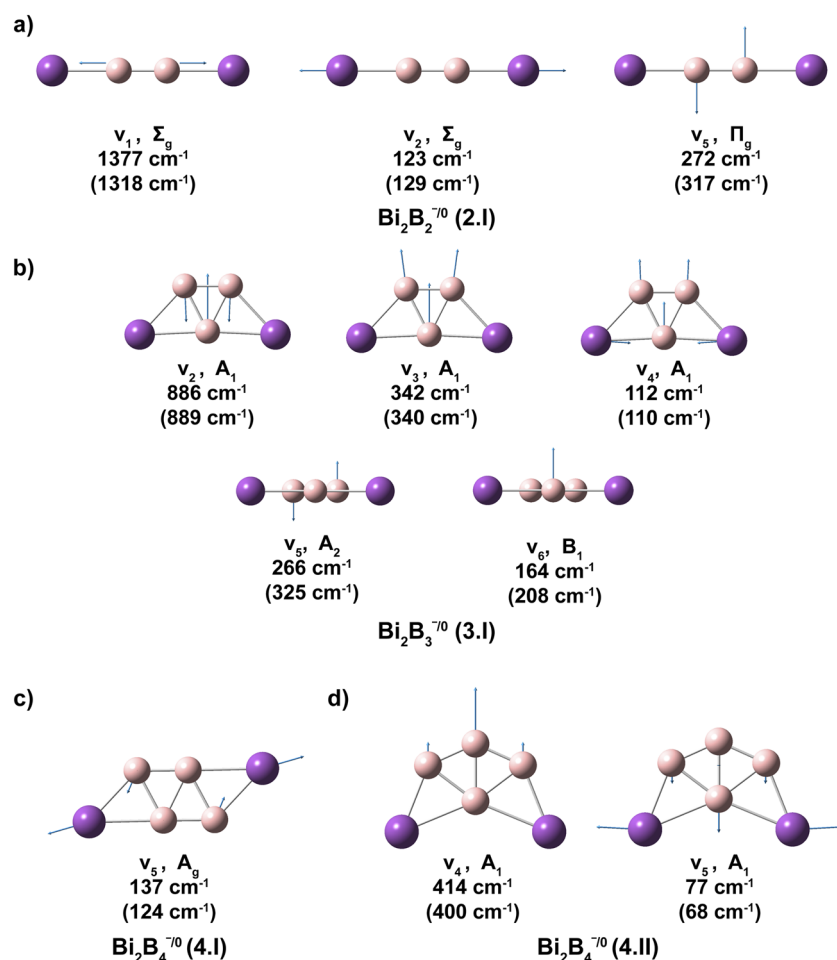


FIG. 7. Displacement vectors and calculated vibrational frequencies of both the anions and neutrals of the observed vibrational modes for (a) $Bi_2B_2^{-/0}$ (2.I), (b) $Bi_2B_3^{-/0}$ (3.I), (c) $Bi_2B_4^{-/0}$ (4.I), and (d) $Bi_2B_4^{-/0}$ (4.II). The vibrational frequencies of the anions with the same vibrational modes are given in the parentheses.

frequencies presented in Table I. The weak vibrational feature at 2.3318 eV (5_0^2 , Fig. 1) is separated from the 0-0 peak by 432 cm^{-1} (Table S1 of the supplementary material), which is assigned as the second quanta of the ν_5 bending mode involving the B atoms [Fig. 7(a)]. The 5_0^1 transition is forbidden by symmetry. This observation yielded a frequency of $216 \pm 12\text{ cm}^{-1}$ for the ν_5 mode, which is in fair agreement with the calculated frequency of 272 cm^{-1} [Fig. 7(a) and Table I]. The FC factors computed for the $^3\Sigma_g^- \leftarrow ^2\Pi_g$ transition were used to generate a simulated spectrum, as compared with the experimental data in Fig. 8(a). The overall good agreement between experiment and theory confirms the linear global minimum for Bi_2B_2^- .

The detachment transition to an electronically excited neutral state ($^1\Delta_g$) was calculated to be 3.05 eV, which was assigned to the observed peak B [Table I and Fig. 1(d)]. There was also an expected $^1\Sigma_g^-$ excited state from the $1\pi_g^2$ final state electron configuration. This state should be lower in energy than the $^1\Delta_g$ state and was assigned to the observed peak A [Table I and Fig. 1(d)]. Unfortunately, this state could not be calculated due to limitations of the computational software.

The calculated ADE for isomer 2.II-a of Bi_2B_2^- is 1.90 eV, which is quite off from peak X at 2.2783 eV. Furthermore, no signal was observed below the X band. The calculated frequencies for isomer 2.II-n (Table SIV of the supplementary material) also do not agree with the experimental values. Therefore, we could rule out the presence of isomer 2.II-a in our experiment, consistent with its relatively high energy.

2. Bi_2B_3^-

The Bi_2B_3^- spectra in Fig. 2 exhibited a sharp band labeled X with only a few weak vibrational transitions, also indicating a small geometry change upon electron detachment. Isomer 3.I-a [Fig. 6(b)] gave a calculated ADE of 2.43 eV, which is in good agreement with the measured value of 2.5805 eV (Table II). The $1a_2$ HOMO of Bi_2B_3^- (Fig. S6b of the supplementary material) is mainly of Bi 6p character with weak Bi-B π bonding and B-B anti-bonding characters, consistent with the minor geometry change between the anion and neutral ground state [Fig. 6(b)] and the short vibrational progression in the PE spectra. Band A is from detachment of an electron from the $5a_1$ orbital (Table II), resulting in a 2A_1 neutral excited state. The calculated VDE for the 2A_1 state was 3.16 eV, which also agrees well with the experimental value (3.21 eV, Table II).

Three totally symmetric vibrational modes (ν_2 , ν_3 , and ν_4) and a bending mode (ν_5) [Fig. 7(b)] were observed in the ground state detachment transition of Bi_2B_3^- . The vibrational frequencies for modes ν_2 , ν_3 , ν_4 , and ν_5 were calculated to be 886 cm^{-1} , 342 cm^{-1} , 112 cm^{-1} , and 266 cm^{-1} , respectively, in reasonable agreement with the measured frequencies (Table II). More pronounced vibrational hot bands were observed in the PE spectra of Bi_2B_3^- (Fig. 2). The three hot bands (hb1–hb3) with lower binding energies than peak X were assigned to 4_1^0 , 5_1^1 , and 6_1^1 , respectively (Table SII of the supplementary material). Mode ν_5 corresponds to an A_2 mode and ν_6 corresponds to a B_1 mode, as shown in Fig. 7(b). In addition, combination bands of the hot band 5_1^1 and ν_4 were also

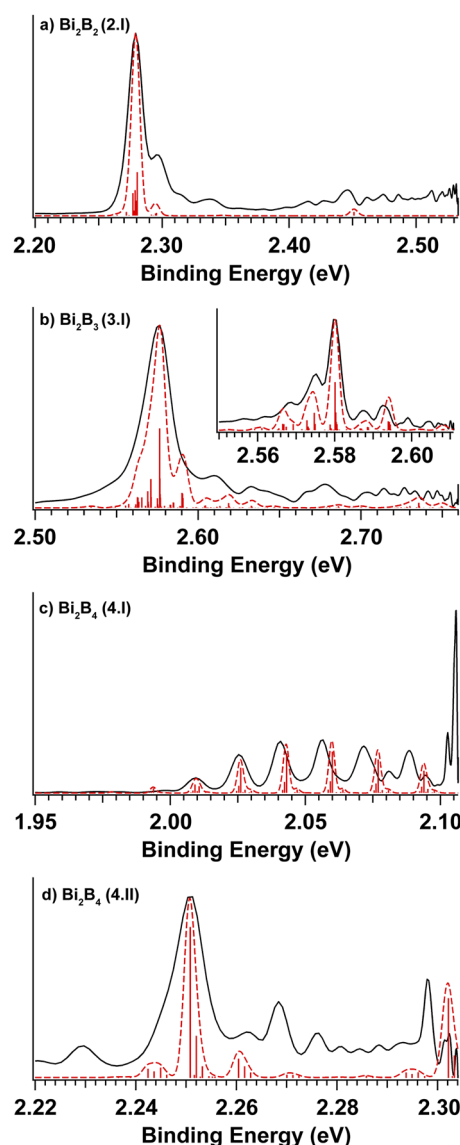


FIG. 8. Comparison of the calculated Franck-Condon factors (vertical lines), using the ezSpectrum v3.0 program⁵³ and the optimized structures of the anions and the neutrals and the computed vibrational frequencies, with the experimental data for (a) Bi_2B_2^- , (b) Bi_2B_3^- , (c) Bi_2B_4^- (4.I), and (d) Bi_2B_4^- (4.II). The vibrational temperatures used were 200 K for Bi_2B_2^- , 300 K for Bi_2B_3^- , and 100 K for Bi_2B_4^- . Gaussian functions were fitted to the FC factors to yield the simulated spectra (dashed curves), which were shifted to align the 0-0 transition to the experiment.

observed, $4_0^1 5_1^1$ and $4_0^2 5_1^1$ (Fig. 2 and Table SII of the supplementary material). From the binding energy of hb1, the vibrational frequency for the ν_4 mode of the anion was estimated to be $107 \pm 12\text{ cm}^{-1}$, in good agreement with the calculated value of 110 cm^{-1} [Fig. 7(b)]. The shoulder next to the 4_0^2 peak was assigned as the 5_0^2 transition (Fig. 2). From the 5_1^1 and the 5_0^2 transitions, the vibrational frequency for the ν_5 mode of the anion was estimated to be $325 \pm 20\text{ cm}^{-1}$, agreeing well with

the computed value [Fig. 7(b)]. Another shoulder labeled hb4 next to the 2_0^1 transition [Fig. 2(c)] was assigned as a $2_0^1 4_1^0$ combination band (Table SII of the [supplementary material](#)). The FC factors were computed for the ground state detachment transitions of isomer 3.I-a and the simulated spectrum is compared with the experimental spectrum in Fig. 8(b). The good agreement between the theoretical results of isomer 3.I and the experimental data provides considerable credence to the C_{2v} global minimum structure of Bi_2B_3^- .

3. Bi_2B_4^-

The complicated PES spectrum of Bi_2B_4^- (Fig. 3) is consistent with the presence of two isomers in the cluster beam, as borne out by the theoretical results predicting two nearly degenerate structures [Fig. 6(c)]. Both the computed electron binding energies and vibrational frequencies of the two isomers are in excellent agreement with the experimental observations, as shown in Table III.

The calculated ADE for the *trans* isomer 4.I-a by removing the electron from the $2a_u$ HOMO was 1.90 eV (Table III), in good agreement with the measured ADE for band X (2.0102 eV). The next detachment channel for isomer 4.I-a involves removal of an electron from the HOMO-1 $1b_g$ orbital, giving rise to a computed VDE of 2.57 eV, in good agreement with the measured VDE of band A (2.69 eV). The $2a_u$ HOMO of the *trans* isomer involves π antibonding interactions between the Bi atoms and the B atoms, as well as π bonding interactions within the B_4 unit (Fig. S6c of the [supplementary material](#)). The removal of the $2a_u$ electron is expected to shorten the Bi-B bond lengths and increase the B-B bond lengths, as borne out by the optimized structure of the neutral *trans* isomer (4.I-n). Thus, a long vibrational progression involving the Bi-B stretching mode [Fig. 7(c)] is expected in the ground state detachment transition, consistent with the extended vibrational progression observed in the high resolution spectra for the X band (Fig. 4). The observed vibrational frequency of $125 \pm 2 \text{ cm}^{-1}$ agrees well with the calculated frequency of 137 cm^{-1} for the Bi-B symmetric stretching mode ν_5 (Table III). In addition, the hot band progression involving the ν_5 mode yielded a frequency for the Bi-B symmetric stretching mode of the anion as $100 \pm 5 \text{ cm}^{-1}$, which is comparable to the calculated value of 124 cm^{-1} [Fig. 7(c)]. The simulated spectrum by using the computed FC factors is compared with the experimental spectrum in Fig. 8(c). The agreement is reasonably good, except for the two peaks above 2.10 eV.

The calculated ADE for isomer 4.II-a by removing the electron in the $2b_1$ HOMO was 2.20 eV, in excellent agreement with the measured ADE for band X' (2.2510 eV), as shown in Table III. The next detachment channel by removing an electron from the $1a_2$ HOMO-1 yielded a computed VDE of 2.66 eV, in good agreement with the observed VDE of band A' (2.77 eV). Hence, bands X' and A' came from the *cis* isomer 4.II-a. The high resolution spectra for band X' revealed two vibrational progressions (Fig. 5). The high frequency mode of $379 \pm 8 \text{ cm}^{-1}$ can be assigned to the B-B stretching mode [ν_4 in Fig. 7(d)] with a computed frequency of 414 cm^{-1} . The lower frequency mode of $67 \pm 7 \text{ cm}^{-1}$ is assigned to the symmetric in-plane bending mode involving the Bi atoms [ν_5 in Fig. 7(d)] with a

computed frequency of 77 cm^{-1} . The HOMO of the *cis* isomer involves π antibonding interactions between the Bi atoms and the B atoms, as well as π bonding interactions within the B_4 unit (Fig. S6d of the [supplementary material](#)). The geometry change in the neutral *cis* isomer [4.II-n in Fig. 6(c)] upon removal of the HOMO electron is consistent with the nature of the HOMO and the observed vibrational activities. The simulated spectrum using the computed FC factors also agrees well with the experimental spectrum [Fig. 8(d)].

The anisotropy parameters (β) were obtained for the 0-0 transitions of all the observed clusters (Fig. S7 of the [supplementary material](#)). The β values are close to 0 for low kinetic energy electrons, indicating their s-wave nature. This observation suggests that the photoelectrons are from π -like orbitals, consistent with the nature of the HOMO in each system (Fig. S6 of the [supplementary material](#)).

B. The structures and bonding in the boron-bismuth binary clusters

To understand the structures of the boron-bismuth binary clusters and the bonding between the Bi atoms and the B_n ($n = 2-4$) motifs, we performed AdNDP analyses,⁵² as shown in Fig. 9. In the case of Bi_2B_3^- , the closed shell anion was used. In all the clusters, the 6s electrons in the Bi atoms are lone-pairs and do not participate in chemical bonding, consistent with the inert 6s orbitals due to the relativistic effects.⁵⁵

1. Bi_2B_2 and Bi_2B_2^-

The two unpaired electrons of the linear Bi_2B_2 result in two weak 1-electron Bi-B π bonds [4c-1e bonds in Fig. 9(a)]. In addition, there are two completely delocalized 4c-2e π bonds, as well as two 2c-2e Bi-B σ bonds and one 2c-2e B-B σ bond. As shown in Fig. 6(a), the Bi-B bond length is 2.140 \AA , while the B-B bond length is 1.549 \AA . The Bi-B bond length in Bi_2B_2 is very similar to the Bi=B double bonds in Bi_2B^- .⁹ There is a small change in the Bi-B and B-B bond lengths between the neutral and the anion. Both the Bi-B and B-B bond lengths in the linear Bi_2B_2 cluster are slightly shorter than the Bi=B and B=B double bond lengths calculated from Pyykko's self-consistent atomic covalent radii of B and Bi.⁵⁶ Hence, the linear Bi_2B_2 species can be approximately described as $\text{Bi}=\text{B}=\text{B}=\text{Bi}$ with strong conjugation effects, giving additional stability for the linear structure.

2. Bi_2B_3 and Bi_2B_3^-

In addition to the two 6s lone pairs [Fig. 9(b)], the AdNDP analyses for the closed shell Bi_2B_3^- cluster revealed four 2c-2e Bi-B σ bonds and one 2c-2e B-B σ bond around the periphery of the planar cluster, as well as one 3c-2e delocalized σ bond within the B_3 motif, one 4c-2e π bond along the Bi-B edges of the cluster, and one 5c-2e delocalized π bond mainly within the B_3 unit. The 3c-2e delocalized σ bond within the B_3 motif is similar to that in the bare B_3 cluster.⁵⁴ The 5c-2e delocalized π bond is also similar to that in the bare B_3 cluster, except the small contributions from the Bi atoms. Hence, the B_3 motif in Bi_2B_3 maintains its double aromaticity.⁵⁴ The B-B bond (1.540 \AA) that is not coordinated to Bi has a bond length similar to that in the bare B_3 cluster. However, the two

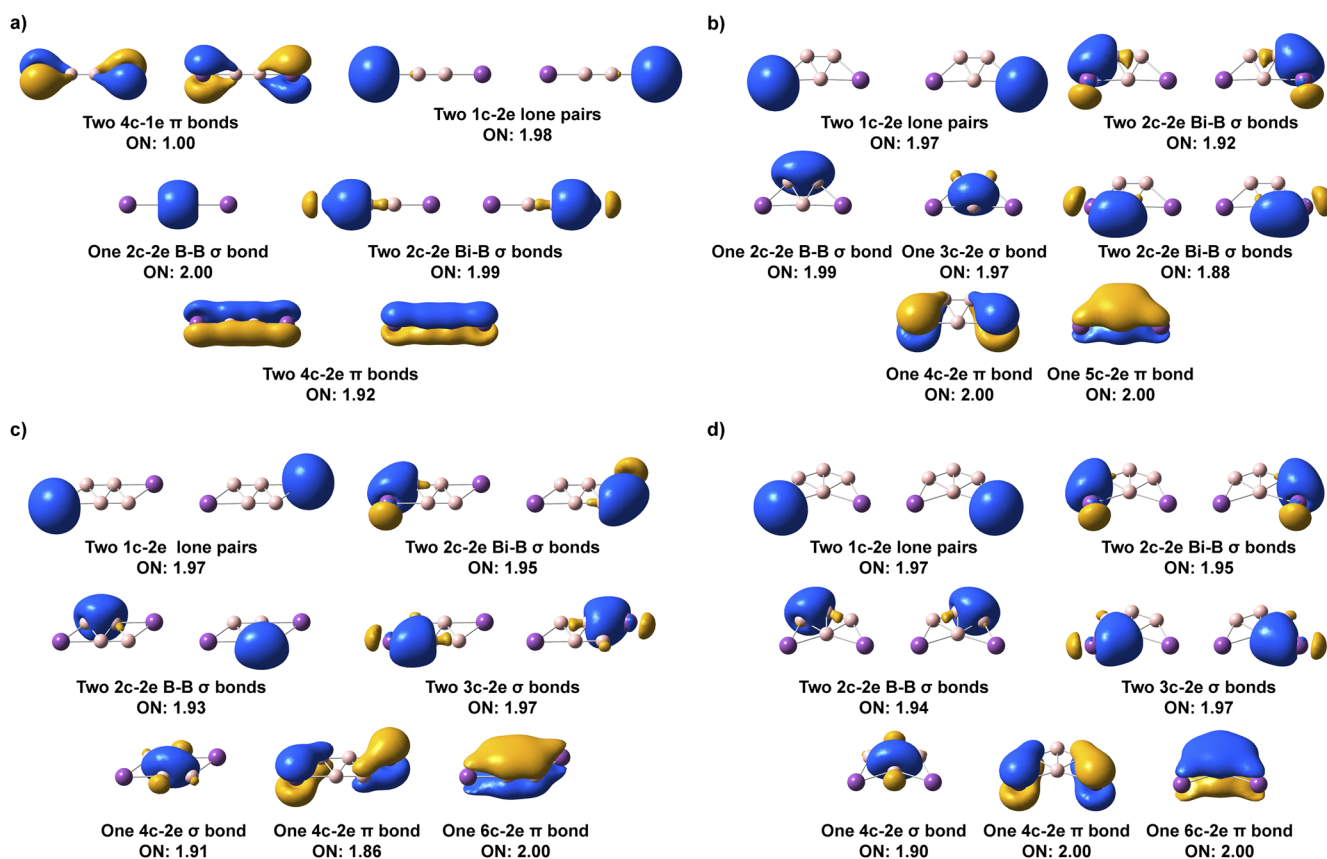


FIG. 9. Chemical bonding analyses of (a) Bi_2B_2 (2.I-n), (b) Bi_2B_3^- (3.I-a), (c) Bi_2B_4 (4.I-n), and (d) Bi_2B_4 (4.II-n) using the AdNDP method.⁵²

B-B bonds (1.710 Å) that are coordinated to Bi are significantly lengthened. The 4c-2e π bond is mainly of Bi $6p_z$ character with weak Bi-B bonding, corresponding to the HOMO of Bi_2B_3^- (Fig. S6b of the [supplementary material](#)). The very small structure change in the neutral Bi_2B_3 cluster upon electron detachment [Fig. 6(b)] is consistent with the weak bonding nature of the 4c-2e π bond.

3. Bi_2B_4 and Bi_2B_4^-

The AdNDP analyses of the two closed-shell neutral Bi_2B_4 isomers are shown in Figs. 9(c) and 9(d), which reveal similar bonding properties in the two structures. In addition to the two 6s lone pairs, each contains four Bi-B σ bonds and two B-B σ bonds around the periphery of the clusters, one 4c-2e delocalized σ bonds within the B_4 motif, one 6c-2e π bond mainly localized on the B_4 unit with minor contributions from the Bi atoms, and one 4c-2e π bond mainly of Bi $6p_z$ character with weak Bi-B bonding. In fact, the bonding in the two Bi_2B_4 isomers is similar to that in Bi_2B_3^- . The B-B bonds that are not coordinated by Bi have bond lengths similar to those in the bare B_4 cluster,⁵⁴ while the B-B bonds that are coordinated by Bi are significantly lengthened in comparison to those in the bare B_4 cluster.

4. Comparison of the structures of B-Bi and other B-group-V binary clusters

It is interesting to note the increase in the B-B bond lengths in the B_3 and B_4 units when they are coordinated by the Bi atoms. The Bi-B bonds weaken the B-B bonds on the edge by breaking the B-B σ bond. The B-B bonds with the Bi coordination only involve delocalized σ and π interactions [Figs. 9(b)–9(d)]. But the Bi-B bond is not strong enough to completely break the B-B bonds. In the B_3N cluster, the strong B-N bond breaks the B-B bond and it becomes linear with a B-N-B configuration.³² The B_3N_2 cluster was studied computationally, suggesting that the N atoms also insert into the B-B bonds and disrupt the B_3 triangle.³³ However, a previous theoretical study showed that P_2B_n clusters exhibit global minimum structures similar to the corresponding Bi_2B_n clusters studied currently.³⁴ A recent study of Bi_2Al_n^- clusters showed that they all have three-dimensional structures due to the weak Al-Al bonds.³⁵ Hence, the competition between the B-M and B-B bonding determines the structures of the M_2B_n clusters. It would be interesting to study the stoichiometric Bi_nB_n clusters, which may provide interesting information about bulk BiB, which was predicted to have similar structures as the other III-V semiconductor materials.

VII. CONCLUSION

We report an experimental and theoretical investigation of a series of Bi_2B_n^- and Bi_2B_n ($n = 2-4$) clusters using high-resolution PE imaging and DFT calculations. Electron affinities and vibrational frequencies of the Bi_2B_n neutral clusters are obtained and compared with the theoretical results. Bi_2B_2^- is found to be linear, while Bi_2B_3^- and Bi_2B_4^- are found to be planar. The B_3 triangle and B_4 rhombus motifs are maintained in the latter, even though the B–B bonds that are coordinated by Bi are significantly weakened. The bonding in the linear Bi_2B_2 cluster can be viewed approximately as $\text{Bi}=\text{B}=\text{Bi}$. The Bi_2B_3^- cluster is found to have C_{2v} symmetry with the two Bi atoms coordinated to the edges of the B_3 triangle. The delocalized σ and π bonds in Bi_2B_3^- are similar to those in the bare B_3 cluster. Two nearly degenerate isomers were found to co-exist in the experiment, consisting of a B_4 rhombus coordinated by the two Bi atoms either in the *trans* or *cis* fashion. The bonding in the two Bi_2B_4^- isomers is similar, both containing a delocalized σ and π bond in the B_4 unit.

SUPPLEMENTARY MATERIAL

See [supplementary material](#) for the binding energies of all the observed vibrational peaks, all the vibrational frequencies of the global minima and a low-lying isomer of Bi_2B_n and Bi_2B_n^- ($n = 2-4$), the anisotropy parameter (β) of the ground state 0–0 detachment transitions, the complete isomers of Bi_2B_n^- ($n = 2-4$) within 1 eV of the global minima, and the valence molecular orbital pictures of the global minima.

ACKNOWLEDGMENTS

This work was supported by the National Science Foundation (Grant No. CHE-1763380). L.F.C. would like to thank Dr. Tian Jian for valuable discussions. G.S.K. was supported by a Philip A. Smith Chemistry Fellowship.

REFERENCES

- I. Vurgaftman, J. R. Meyer, and L. R. Ram-Mohan, *J. Appl. Phys.* **89**, 5815 (2001).
- D. Madouri and M. Ferhat, *Phys. Status Solidi B* **242**, 2856 (2005).
- S. Cui, W. Feng, H. Hua, Z. Feng, and Y. Wang, *Comput. Mater. Sci.* **47**, 968 (2010).
- B. G. Yalcin, S. Bagci, M. Ustundag, and M. Aslan, *Comput. Mater. Sci.* **98**, 136 (2015).
- S. Bagci and B. G. Yalcin, *J. Phys. D: Appl. Phys.* **48**, 475304 (2015).
- R. P. Shahri and A. Akhtar, *Chin. Phys. B* **26**, 093107 (2017).
- J. S. Lu, S. H. Su, M. C. Yang, X. T. Wen, J. Z. Xie, and M. D. Su, *Organometallics* **35**, 3924 (2016).
- T. Jian, G. V. Lopez, and L. S. Wang, *J. Phys. Chem. B* **120**, 1635 (2016).
- T. Jian, L. F. Cheung, T. T. Chen, and L. S. Wang, *Angew. Chem., Int. Ed.* **56**, 9551 (2017).
- H. J. Zhai, L. S. Wang, A. N. Alexandrova, and A. I. Boldyrev, *J. Chem. Phys.* **117**, 7917 (2002).
- H. J. Zhai, B. Kiran, J. Li, and L. S. Wang, *Nat. Mater.* **2**, 827 (2003).
- A. N. Alexandrova, A. I. Boldyrev, H. J. Zhai, and L. S. Wang, *Coord. Chem. Rev.* **250**, 2811 (2006).
- E. Oger, N. R. M. Crawford, R. Kelting, P. Weis, M. M. Kappes, and R. Ahlrichs, *Angew. Chem., Int. Ed.* **46**, 8503 (2007).
- A. P. Sergeeva, I. A. Popov, Z. A. Piazza, W. L. Li, C. Romanescu, L. S. Wang, and A. I. Boldyrev, *Acc. Chem. Res.* **47**, 1349 (2014).
- M. R. Fagiani, X. Song, P. Petkov, S. Debnath, S. Gewinner, W. Schöllkopf, T. Heine, A. Fielicke, and K. R. Asmis, *Angew. Chem., Int. Ed.* **56**, 501 (2017).
- L. S. Wang, *Int. Rev. Phys. Chem.* **35**, 69 (2016).
- Z. A. Piazza, H. S. Hu, W. L. Li, Y. F. Zhao, J. Li, and L. S. Wang, *Nat. Commun.* **5**, 3113 (2014).
- A. J. Mannix, Z. Zhang, N. P. Guisinger, B. I. Yakobson, and M. C. Hersam, *Nat. Nanotechnol.* **13**, 444 (2018).
- H. J. Zhai, Y. F. Zhao, W. L. Li, Q. Chen, H. Bai, H. S. Hu, Z. A. Piazza, W. J. Tian, H. G. Lu, Y. B. Wu, Y. W. Mu, G. F. Wei, Z. P. Liu, J. Li, S. D. Li, and L. S. Wang, *Nat. Chem.* **6**, 727 (2014).
- C. Romanescu, A. P. Sergeeva, W. L. Li, A. I. Boldyrev, and L. S. Wang, *J. Am. Chem. Soc.* **133**, 8646 (2011).
- T. R. Galeev, C. Romanescu, W. L. Li, L. S. Wang, and A. I. Boldyrev, *Angew. Chem., Int. Ed.* **51**, 2101 (2012).
- C. Romanescu, T. R. Galeev, W. L. Li, A. I. Boldyrev, and L. S. Wang, *Acc. Chem. Res.* **46**, 350 (2013).
- I. A. Popov, T. Jian, G. V. Lopez, A. I. Boldyrev, and L. S. Wang, *Nat. Commun.* **6**, 8654 (2015).
- W. L. Li, T. Jian, X. Chen, H. R. Li, T. T. Chen, X. M. Luo, S. D. Li, J. Li, and L. S. Wang, *Chem. Commun.* **53**, 1587 (2017).
- W. L. Li, T. Jian, X. Chen, T. T. Chen, G. V. Lopez, J. Li, and L. S. Wang, *Angew. Chem., Int. Ed.* **55**, 7358 (2016).
- T. Jian, W. L. Li, X. Chen, T. T. Chen, G. V. Lopez, J. Li, and L. S. Wang, *Chem. Sci.* **7**, 7020 (2016).
- W. L. Li, X. Chen, T. Jian, T. T. Chen, J. Li, and L. S. Wang, *Nat. Rev. Chem.* **1**, 0071 (2017).
- W. L. Li, H. S. Hu, Y. F. Zhao, X. Chen, T. T. Chen, T. Jian, L. S. Wang, and J. Li, *Sci. Sin.: Chim.* **48**, 98 (2018).
- W. L. Li, T. T. Chen, D. H. Xing, X. Chen, J. Li, and L. S. Wang, *Proc. Natl. Acad. Sci. U. S. A.* **115**, E6972 (2018).
- K. R. Asmis, T. R. Taylor, and D. M. Neumark, *Chem. Phys. Lett.* **295**, 75 (1998).
- K. R. Asmis, T. R. Taylor, and D. M. Neumark, *J. Chem. Phys.* **111**, 8838 (1999).
- K. R. Asmis, T. R. Taylor, and D. M. Neumark, *J. Chem. Phys.* **111**, 10491 (1999).
- W. Cui, C. Wang, J. Shao, and X. Zhu, *Int. J. Quantum Chem.* **113**, 2251 (2013).
- C. He, J. Shao, R. Shi, and X. Zhu, *Comput. Theor. Chem.* **964**, 121 (2011).
- Z. Sun, H. G. Xu, G. Feng, X. L. Xu, and W. J. Zheng, *Chem. Phys. Lett.* **615**, 56 (2014).
- I. Leon, Z. Yang, and L. S. Wang, *J. Chem. Phys.* **138**, 184304 (2013).
- Z. Yang, I. Leon, and L. S. Wang, *J. Chem. Phys.* **139**, 021106 (2013).
- I. León, Z. Yang, H. T. Liu, and L. S. Wang, *Rev. Sci. Instrum.* **85**, 083106 (2014).
- J. Czekner, L. F. Cheung, E. L. Johnson, R. C. Fortenberry, and L. S. Wang, *J. Chem. Phys.* **148**, 044301 (2018).
- B. Dick, *Phys. Chem. Chem. Phys.* **16**, 570 (2014).
- A. Sanov and R. Mabbs, *Int. Rev. Phys. Chem.* **27**, 53 (2008).
- J. Clark, S. T. Call, D. E. Austin, and J. C. Hansen, *J. Phys. Chem. A* **114**, 6534 (2010).
- B. B. Averkiev, S. Call, A. I. Boldyrev, L. M. Wang, W. Huang, and L. S. Wang, *J. Phys. Chem. A* **112**, 1873 (2008).
- S. T. Call, D. Y. Zubarev, and A. I. Boldyrev, *J. Comput. Chem.* **28**, 1177 (2007).
- S. Kirkpatrick, C. D. Gelatt, and M. P. Vecchi, *Science* **220**, 671 (1983).
- J. P. Perdew, K. Burke, and M. Ernzerhof, *Phys. Rev. Lett.* **77**, 3865 (1996).
- P. J. Hay and W. R. Wadt, *J. Chem. Phys.* **82**, 270 (1985).
- J. M. Tao, J. P. Perdew, V. N. Staroverov, and G. E. Scuseria, *Phys. Rev. Lett.* **91**, 146401 (2003).
- K. A. Peterson, *J. Chem. Phys.* **119**, 11099 (2003).

⁵⁰R. A. Kendall, T. H. Dunning, Jr., and R. J. Harrison, *J. Chem. Phys.* **96**, 6796 (1992).

⁵¹M. J. Frisch, G. W. Trucks, H. B. Schlegel, G. E. Scuseria, M. A. Robb, J. R. Cheeseman, G. Scalmani, V. Barone, B. Mennucci, G. A. Petersson, H. Nakatsuji, M. Caricato, X. Li, H. P. Hratchian, A. F. Izmaylov, J. Bloino, G. Zheng, J. L. Sonnenberg, M. Hada, M. Ehara, K. Toyota, R. Fukuda, J. Hasegawa, M. Ishida, T. Nakajima, Y. Honda, O. Kitao, H. Nakai, T. Vreven, J. A. Montgomery, Jr., J. E. Peralta, F. Ogliaro, M. Bearpark, J. J. Heyd, E. Brothers, K. N. Kudin, V. N. Staroverov, R. Kobayashi, J. Normand, K. Raghavachari, A. Rendell, J. C. Burant, S. S. Iyengar, J. Tomasi, M. Cossi, N. Rega, J. M. Millam, M. Klene, J. E. Knox, J. B. Cross, V. Bakken, C. Adamo, J. Jaramillo, R. Gomperts, R. E. Stratmann, O. Yazyev, A. J. Austin, R. Cammi, C. Pomelli,

J. W. Ochterski, R. L. Martin, K. Morokuma, V. G. Zakrzewski, G. A. Voth, P. Salvador, J. J. Dannenberg, S. Dapprich, A. D. Daniels, Ö. Farkas, J. B. Foresman, J. V. Ortiz, J. Cioslowski, and D. J. Fox, gaussian 09, Revision C.1, Gaussian, Inc., Wallingford, CT, 2009.

⁵²D. Y. Zubarev and A. I. Boldyrev, *Phys. Chem. Chem. Phys.* **10**, 5207 (2008).

⁵³V. A. Mozhayskiy and A. I. Krylov, ezSpectrum, <http://iopenshell.usc.edu/downloads>, 2009.

⁵⁴Z. H. Zhai, L. S. Wang, A. N. Alexandrova, A. I. Boldyrev, and V. G. Zakrzewski, *J. Phys. Chem. A* **107**, 9319 (2003).

⁵⁵P. Pyykkö, *Chem. Rev.* **88**, 563 (1988).

⁵⁶P. Pyykkö, *J. Phys. Chem. A* **119**, 2326 (2015).